PLANT SCIENCES

An auxin-regulable oscillatory circuit drives the root clock in *Arabidopsis*

Juan Perianez-Rodriguez[1]*, Marcos Rodriguez[2†], Marco Marconi[1†], Estefano Bustillo-Avendaño[1], Guy Wachsman[3], Alvaro Sanchez-Corrionero[1], Hugues De Gernier[4,5], Javier Cabrera[1], Pablo Perez-Garcia[1], Inmaculada Gude[1], Angela Saez[1], Laura Serrano-Ron[1], Tom Beeckman[4,5], Philip N. Benfey[3], Alfonso Rodríguez-Patón[2], Juan Carlos del Pozo[1], Krzysztof Wabnik[1‡], Miguel A. Moreno-Risueno[1‡]

In *Arabidopsis*, the root clock regulates the spacing of lateral organs along the primary root through oscillating gene expression. The core molecular mechanism that drives the root clock periodicity and how it is modified by exogenous cues such as auxin and gravity remain unknown. We identified the key elements of the oscillator (AUXIN RESPONSE FACTOR 7, its auxin-sensitive inhibitor IAA18/POTENT, and auxin) that form a negative regulatory loop circuit in the oscillation zone. Through multilevel computer modeling fitted to experimental data, we explain how gene expression oscillations coordinate with cell division and growth to create the periodic pattern of organ spacing. Furthermore, gravistimulation experiments based on the model predictions show that external auxin stimuli can lead to entrainment of the root clock. Our work demonstrates the mechanism underlying a robust biological clock and how it can respond to external stimuli.

INTRODUCTION

Both plants and animals can regulate patterning through developmental clocks that involve oscillating gene expression (*1*). In *Arabidopsis thaliana*, the root clock determines organ spacing along the primary root axis by establishing prebranch sites (PBS) through oscillating gene expression approximately every 6 hours (*2*). However, periodicity of the root clock can vary under specific environmental conditions or by supplementation with the phytohormone auxin (*2*–*4*). Oscillations in gene expression occur as propagating waves in the oscillation zone (OZ) in two opposite phases: in-phase and antiphase based on expression of the *DR5::Luciferase* auxin response reporter (*2*). When expression of in-phase genes is activated in the OZ, the expression of antiphase genes is repressed and vice versa.

At the cellular level, PBS formation is interpreted as priming of pericycle cells to specify lateral root (LR) founder cells, which is a prepatterning stage (*5*). Subsequently, LRs originate from PBS (*2*) through division of founder cells (*1*, *5*–*9*).

Programmed cell death has been proposed to release auxin into the OZ to control periodicity of the root clock (*4*). In addition, auxin derived from the lateral root cap (LRC) and the Aux/IAA factor IAA28 regulate *DR5::Luciferase* oscillations and PBS formation (*3*, *4*, *10*). However, how periodicity of the in-phase and antiphase oscillations is established in the OZ to determine PBS spacing is not resolved.

RESULTS AND DISCUSSION

To gain further insight into the root clock mechanism, we performed a mutagenesis screen in plants carrying *DR5::Luciferase* in combination with markers for subsequent LR organogenesis [*pWOX5::ER-YFP* and *pSCR::ER-GFP* (*11*)]. From this screen, we identified a mutant with increased expression of *DR5::Luciferase* in the OZ as well as PBS distributed throughout the primary root axis without regular spacing (Fig. 1A). Time course analyses of in-phase gene oscillations in the mutant showed a persistent signal in the OZ (movies S1 and S2) without the typical 6-hour oscillatory behavior, thereby causing abnormal PBS spacing (Fig. 1, B and C). Introgression of a specific marker for LR founder cells (*12*) in this mutant showed that most pericycle cells had been specified as founder cells (Fig. 1D). Because of this increased capacity to form PBS and LR founder cells, we named this mutant *potent*. In summary, root clock function is impaired in *potent*, which results in more priming and abnormal LR prepatterning events.

Mapping of the *potent* mutation showed a change of cytosine to thymine in the coding sequence of the *IAA18* gene, causing the substitution of proline 102 by leucine in the DII domain (fig. S1, A to D, and data file S1). Mutations in conserved DII domain prolines have been associated with auxin insensitivity and increased stability of the Aux/IAA proteins, resulting in dominant mutations (fig. S1E) (*13*–*15*). The expression of the *iaa18/potent* allele (IAA18P102L) under an estradiol-inducible promoter showed increased numbers of LR founder cells with increasing doses of estradiol (Fig. 1E), thus confirming the regulation of priming by IAA18/POTENT activity. Aux/IAA proteins are thought to act redundantly during development (*13*, *16*). It is possible that IAA18/POTENT may function redundantly with other Aux/IAAs; however, IAA26, the closest homolog of IAA18/POTENT, is not expressed at detectable levels in the OZ (*17*).

Next, we determined that founder cells in *iaa18/potent* mutant did not undergo further development (fig. S2A), explaining the absence of LRs in this mutant (fig. S2, B and C). Other Aux/IAA proteins regulate LR founder cell division (*11*, *18*, *19*), so we reasoned

[1]Centro de Biotecnología y Genómica de Plantas (Universidad Politécnica de Madrid–Instituto Nacional de Investigación y Tecnología Agraria y Alimentaria). Campus de Montegancedo, Pozuelo de Alarcón, 28223 Madrid, Spain. [2]Departamento de Inteligencia Artificial, ETSIINF, Universidad Politécnica de Madrid, 28040 Madrid, Spain. [3]Department of Biology, Howard Hughes Medical Institute, Duke University, Durham, NC 27708, USA. [4]Ghent University, Department of Plant Biotechnology and Bioinformatics, Technologiepark 71, 9052 Ghent, Belgium. [5]VIB Center for Plant Systems Biology, Technologiepark 71, 9052 Ghent, Belgium.
*Present address: Departamento de Biología y Geología, Física y Química Inorgánica, Universidad Rey Juan Carlos, E-28933 Móstoles, Spain.
†These authors contributed equally to this work.
‡Corresponding author. Email: k.wabnik@upm.es (K.W.); miguelangel.moreno@upm.es (M.A.M.-R.)

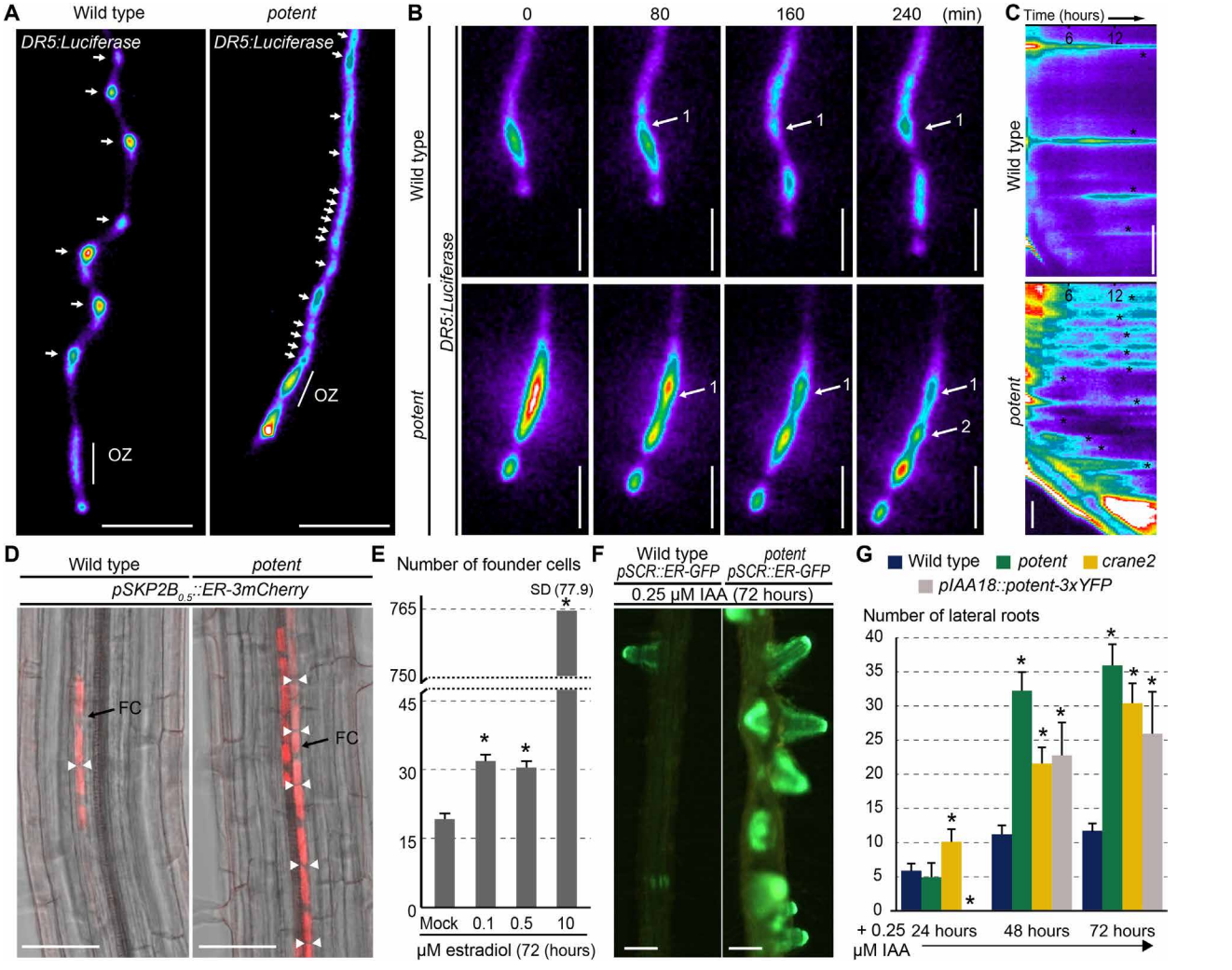

Fig. 1. The IAA18/POTENT factor regulates the root clock oscillations and LR priming. (**A** and **B**) *DR5::Luciferase* oscillations lack the typical oscillatory behavior causing abnormal PBS spacing in *iaa18/potent* mutant. Arrows: PBS. (**C**) Kymograph showing increased PBS production in *iaa18/potent* roots. Asterisks: PBS. Note that not all PBS are maintained over time. (**D** and **E**) *iaa18/potent* allele overproduces founder cells (FC) as shown by (D) confocal microscopy and (E) the quantification of the FC marker *pSKP2B0.5::ER-3mCherry* in a *iaa18/potent* (IAA18P102L) estradiol-inducible line (*pER8::iaa18/potent*). Arrowheads: FC limits. (**F**) Altered positioning of LRs in *iaa18/potent* mutant. (**G**) Quantification of LR formation in *iaa18/potent*, in *iaa18/potent* allele (IAA18P102L) expressed under its regulatory regions, and in an alternative mutant allele (*crane2*). (A to D) Seven days post imbibition (dpi). (E to G) Seedlings were treated at 4 dpi. Scale bars, 5 mm (A), 1 mm (B), 50 µm (D), and 0.1 mm (F). *$P < 0.001$ by general linear model (GLM)/least significant difference (LSD). *n* per sample: ≥10 (E) and ≥20 (G). Error bars, SD.

that IAA18/POTENT might function redundantly during LR initiation. Using an auxin concentration (0.25 µM) that does not alter prepatterning in the wild type (fig. S3A) but promotes LR initiation, we observed production of LRs in *iaa18/potent* roots (Fig. 1F). This confirms that LRs can be initiated through alternative Aux/IAA combinations even in the presence of the *iaa18/potent* mutated protein. Furthermore, we observed increased production of LRs with reduced or no spacing in *iaa18/potent* mutant as well as when *iaa18/potent* (IAA18P102L) was expressed under its native regulatory regions and in *crane2* (Fig. 1E), which harbors an alternative mutation in the DII domain of *IAA18* (fig. S1E) (*20*).

When we treated the *iaa18/potent* (IAA18P102L) estradiol-inducible line with low estradiol doses and with an auxin concentration over the threshold (0.25 µM) that induces founder cell specification, we observed an additive effect of *iaa18/potent* allele with auxin in founder cell specification and LR formation (fig. S3B). In contrast, higher estradiol doses prevented development of the numerous induced founder cells (fig. S3C), thus inhibiting LR initiation (fig. S3B). These results indicate that priming and LR founder specification are highly sensitive to IAA18/POTENT levels, placing IAA18/POTENT in a central role in prepatterning.

Consistent with this role, we found that the wild-type IAA18/POTENT-Luciferase protein was present in the OZ and PBS, while in the *iaa18/potent* allele (IAA18P102L-Luciferase), the protein was primarily stabilized in the OZ and shootward regions where priming is typically observed (fig. S4A). IAA18/POTENT-YFP displayed both nuclear and cytoplasmic localization in the endodermis and pericycle cells of the OZ, whereas the *iaa18/potent* mutation (IAA18P102L-YFP) caused accumulation in the nucleus (fig. S4, B and C). Supplementation with auxin caused degradation of

wild-type IAA18/POTENT-YFP, whereas no change in *iaa18/potent* (IAA18P102L-YFP) protein levels was observed (fig. S4, D and E), consistent with observations for other Aux/IAA DII domain mutants (*14*, *15*). The absence of the *DR5::Luciferase* oscillatory behavior in *iaa18/potent* mutant is, therefore, associated with the reduced capacity of this factor to be degraded by auxin.

Aux/IAA proteins are inhibitors of auxin response factors (ARFs) (*21*). ARF7 is a member of the ARF family that has been shown to be involved in PBS formation (*2*), root hydropatterning (*22*), and LR initiation (*23*). Furthermore, *ARF7* transcripts tend to oscillate in antiphase to *DR5::Luciferase* (*2*). Analysis of ARF7 under its native regulatory regions using recombineering (*24*) showed a predominant nuclear localization coinciding, at the maximum ARF7 levels, with the beginning of the OZ (fig. S5). Nucleocytoplasmic partitioning of ARF7 has been associated with auxin responsiveness (*25*), suggesting that transcriptional regulation mediated by ARF7 would be active primarily in the OZ. In addition, we observed that ARF7 levels fluctuated in the OZ over time (fig. S5). Time course analyses of *DR5::Luciferase* in a loss-of-function *arf7-1* mutant showed enhanced signal in the OZ (Fig. 2A) and absence of the characteristic oscillations (Fig. 2B and movie S3), resulting in more PBS formation (Fig. 2C). Furthermore, introgression of the LR founder cell marker in *arf7-1* mutant showed that many pericycle cells were specified as founder cells, indicating more priming events as compared with the control (Fig. 2D). Many of these founder cells in *arf7-1* mutant did not develop into LRs, even upon 0.25 μM auxin supplementation, which is consistent with a requirement for the transcriptional activating function of ARF7 during LR initiation (*23*), and the observation that not all PBS in *arf7-1* roots are maintained over time (Fig. 2C). In conclusion, the root clock function in *arf7-1* mutant is impaired in the OZ, resulting in altered prepatterning, which phenocopied that of *iaa18/potent* mutant.

As both *iaa18/potent* and *arf7-1* roots showed similar alterations in LR prepatterning and ARF7 and IAA18/POTENT interacted in yeast (fig. S6A), we hypothesized that they could form heterodimers in *Arabidopsis*. To test this hypothesis, we fused these proteins to the half moieties of split-luciferase and expressed them under their own promoters. Reconstitution of split-luciferase has been shown to report functional interactions spatially (*26*). We observed reconstitution of the luciferase signal demonstrating IAA18/POTENT and ARF7 dimerization in the OZ and shootward priming regions (Fig. 2E). No luciferase reconstitution was observed in controls (fig. S6, B to D). Luciferase reconstitution between *iaa18/potent* (IAA18P102L) and ARF7 showed increased signal in the OZ and priming regions, as compared with wild-type IAA18/POTENT, indicating heterodimer accumulation in *iaa18/potent* roots (Fig. 2E and fig. S6E). This accumulation correlates with an increase in *DR5::Luciferase* expression in the OZ and absence of the oscillatory behavior, suggesting that heterodimer formation derepresses the oscillations, probably because IAA18/POTENT inhibits ARF7 activity in the OZ.

ARF7 function during hydropatterning requires posttranslational modification by SUMOylation, which occurs in the presence of auxin and mediates ARF7 interaction with IAA3 (*22*). SUMOylation of ARF7 does not appear to be required for interaction with IAA14/SOLITARY-ROOT during LR initiation (*22*). Because bacteria lack SUMOylation, we tested the interaction using proteins produced in bacteria and found that IAA18/POTENT (or *iaa18/potent*-IAA18P102L) and ARF7 interaction does not require SUMOylation (Fig. 2F).

To understand regulation of the oscillation phases by IAA18/POTENT and ARF7, we performed RNA sequencing (RNA-seq) on samples from the OZ taken at the minimum of *DR5::Luciferase* expression for wild type and, simultaneously, for *arf7-1* and *iaa18/potent* mutants regardless of *DR5::Luciferase* expression to avoid bias (fig. S7A) (*9*). Analysis of differentially expressed genes in *arf7-1* and *iaa18/potent* mutants (compared with wild type; data file S2) showed large overlap, with ~65% deregulated genes in common (Fig. 2G). Of the deregulated oscillating genes, we found that most of the in-phase genes were activated in *arf7-1* and *iaa18/potent* mutants, whereas most antiphase genes were repressed (Fig. 2H). When we overexpressed ARF7, we observed repression of in-phase genes in the OZ, which would return to levels similar to wild type by the introgression of *iaa18/potent* allele (Fig. 2I). These results reveal that ARF7 acts as a repressor in the regulation of in-phase oscillating genes, and this function is modulated by IAA18/POTENT.

To investigate upstream regulation of IAA18/POTENT and IAA28 function, we crossed *iaa28-1* allele, which harbors a mutation in the DII domain causing auxin insensitivity (*10*), with *iaa18/potent* allele and introgressed markers. We observed that increased expression of *DR5::Luciferase* in the OZ caused by *iaa18/potent* mutant did not occur in *iaa28-1* mutant (Fig. 2J), suggesting epistasis. When we investigated expression of *DR5::Luciferase* in the double-mutant *arf7-1 iaa28-1*, we observed expression levels similar to those in *iaa28-1* mutant. We conclude that ARF7 repression of in-phase genes and its inhibition by IAA18/POTENT require activation by auxin. We interpret these results as the existence of two separate signaling mechanisms for auxin that determine two antagonistic actions. IAA28 signaling, which comes first and activates auxin responses, would define the intensity or amplitude of the oscillations. Next, IAA18 signaling would act by repressing gene expression to define the oscillations and their periodicity through negative feedback.

In our transcriptomic analysis, we also investigated categories of genes involved in root clock function (fig. S7B). Several of these such as cell wall remodeling and vesicle trafficking have been previously shown to participate in the root clock (*9*). We found up-regulation of the auxin biosynthetic branch shared with glucosinolate production in *arf7-1* and *iaa18/potent* mutants (fig. S7C). Indole-3-butyric acid conversion to auxin in the LRC has been associated with root clock function and would require auxin transport to the epidermis (*27*). However, it is unknown whether local auxin biosynthesis is required for the root clock mechanism. We investigated auxin content using the auxin biosensor R2D2, in which the ratio between the red fluorescent protein and yellow fluorescent protein (YFP) is a proxy for auxin concentration (*28*). We found high variability in the OZ of control plants. Notably, *arf7-1* and *iaa18/potent* mutants had more auxin in the OZ, while the ARF7 overexpression line had lower levels (Fig. 3A). LRC-derived auxin has been associated with gene expression oscillations through the turnover of DR5 stripes (*6*). We found that DR5 stripes in *iaa18/potent* mutant disappeared at the same rate as control plants, although there appear to be more stripes in *iaa18/potent* mutant (Fig. 3B). These results indicate that IAA18/POTENT and ARF7 are unlikely to regulate LRC-derived auxin, although modulation of auxin levels in the OZ by these factors could be part of the mechanism of the root clock.

As auxin levels change in the OZ, we asked whether auxin feeds back on *IAA18/POTENT* and *ARF7* expression or their protein levels. When we used the minimum local auxin concentration (0.01 μM)

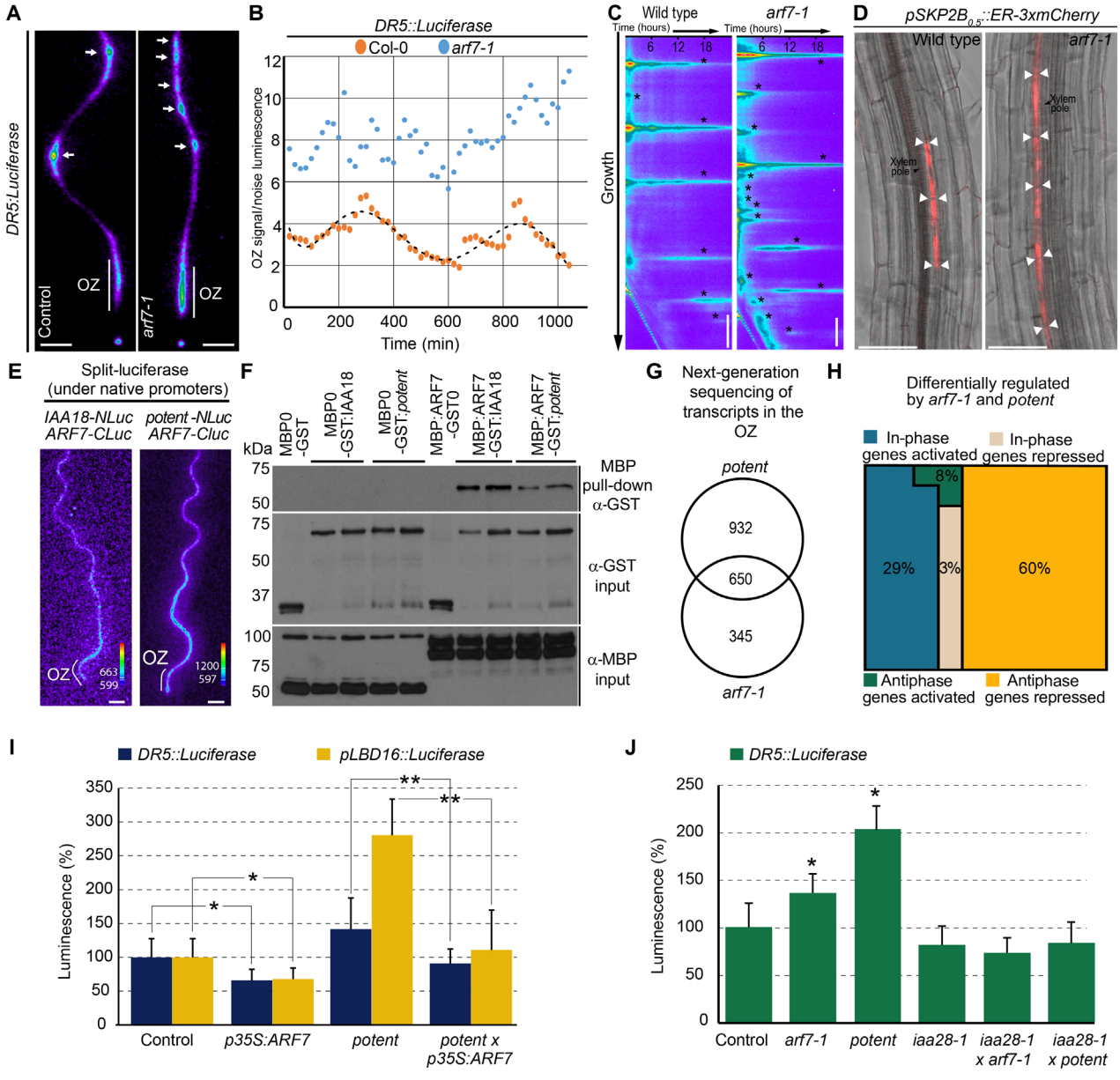

Fig. 2. ARF7 and IAA18/POTENT jointly regulate the root clock. (**A** and **B**) Altered *DR5::Luciferase* oscillations and PBS spacing are observed in the loss-of-function mutant *arf7-1*. Arrows: PBS. Dashed line: Polynomial regression. (**C**) Kymograph showing increased PBS production in *arf7-1* roots. Asterisks: PBS. Note that not all PBS are maintained over time. (**D**) Confocal microscopy images of the FC marker *pSKP2B0.5::ER-3xmCherry* in *arf7-1* roots show FC overspecification. Arrowheads: FC limits. (**E**) Split-luciferase signal reconstitution shows heterodimerization of AUXIN RESPONSE FACTOR 7 (ARF7) and IAA18/POTENT or *iaa18/potent* (IAA18P102L) in the OZ and shootward priming regions. (**F**) Pull-down of ARF7 and IAA18/POTENT or *iaa18/potent* (IAA18P102L) expressed in *Escherichia coli*. (**G** and **H**) RNA-seq reveals (G) common differentially expressed genes (DEG) in *arf7-1* and *iaa18/potent* mutants and (H) directional regulation of in-phase (activated) and antiphase (repressed) genes. (**I** and **J**) Quantification of *DR5::Luciferase* and *pLBD6::Luciferase* in the OZ. *LBD16* is an in-phase DEG. Experiments were performed at 7 dpi. Scale bars, 2 mm (A), 1 mm (C and E), and 50 μm (D). *$P < 0.05$, **$P < 0.001$ by GLM/LSD. *n* per sample: ≥20 (I) and ≥10 (J). Error bars, SD.

capable of mimicking an oscillation (*2*), we did not observe changes in *iaa18/potent* levels (Fig. 3C), whereas IAA18/POTENT-YFP protein levels decreased after 3 hours (Fig. 3D). Next, we tested an auxin concentration (1 μM) that induces founder cell specification. We observed increased transcription starting at 1 hour, while IAA18/POTENT-YFP protein levels decreased after 3 hours (Fig. 3, C and D). Intriguingly, both 0.01 and 1 μM auxin treatments produced a similar decrease in IAA18/POTENT-YFP levels at 3 hours, indicating the existence of a buffering mechanism. In contrast, *ARF7* transcription and its protein levels did not change when the higher auxin concentration was tested (Fig. 3E).

To understand the dynamics of IAA18/POTENT and ARF7 circuit in pattern formation (Fig. 4A), we built a computer model of LR priming leading to PBS formation based on parameters inferred from the experimental data (see data file S3 for details). In addition to using experimentally derived model parameters, we performed a

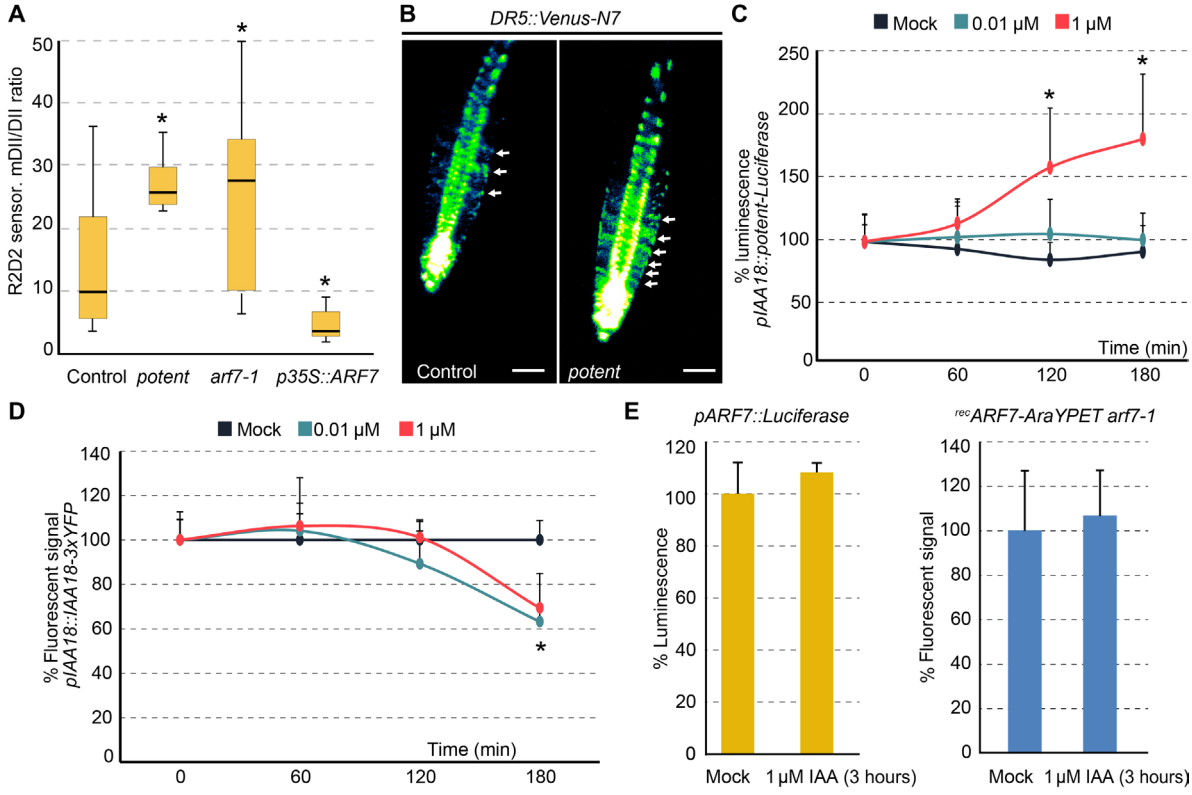

Fig. 3. ARF7 and IAA18/POTENT regulate auxin, and IAA18/POTENT levels are regulated by auxin. (**A**) Quantification of auxin in the OZ epidermis of *arf7-1* and *iaa18/potent* roots using the R2D2 biosensor. (**B**) Stripes of *DR5::VENUS-N7* in control and *iaa18/potent* mutant. Scale bars, 50 µm. (**C**) *IAA18/POTENT* expression in the OZ is activated by auxin. (**D**) IAA18/POTENT levels in the OZ change in response to auxin supplementation. Note that IAA18/POTENT levels are the result of synthesis and degradation. (**E**) *ARF7* expression and ARF7 protein levels in the OZ do not respond to auxin supplementation. Experiments were performed at 7 dpi. *$P < 0.05$ by generalized linear model (GzLM) (A), GLM/LSD (C and D), and Student's *t* test. (E). *n* per sample: ≥10 (A), ≥5 (C and D), and € ≥ 12. Error bars, boxplot whiskers (A) and SD (C to E).

sensitivity analysis and found that the ARF7-IAA18 circuit was most sensitive to ARF7 synthesis rates as well as auxin turnover. These findings are consistent with the importance of ARF7 in the regulation of the oscillatory behavior and PBS formation as indicated by experimental observations. Also, the predicted importance of auxin homeostasis in the ARF7-IAA18 circuit can explain why the excess of auxin in the OZ can override the system and cause induction of LRs (*29*). The model tracks the growth of xylem pole pericycle or pericycle in time and space as priming occurs in these tissues (Fig. 4, B to D) (*6*, *25*, *27*). We found that the model requires an additional hypothetical factor (F) in phase or activated by auxin to explain the observed buffering of IAA18/POTENT protein degradation in the OZ when roots were treated with different auxin concentrations (fig. S8). Predictions suggest that this new component modulates ARF7-IAA18/POTENT heterodimerization, creating an auxin-dependent feedback loop, which promotes auxin response (Fig. 4A).

The model simulations showed a dynamic wave of DR5/in-phase genes originating at the basal meristem and moving shootward with a wavelength of approximately 15 cells (Fig. 4, B and E, and movie S4), which coincides with the region previously described as the OZ. This demonstrates that the propagating waves of gene expression are an emergent property of this system and carry positional information. Oscillations appeared in the simulations every 5 to 6 hours (Fig. 4H), which is in agreement with experimental observations (*2*). When maxima in DR5/in-phase gene expression were associated with LR priming in the model, as in the experimental observations (*2*), the simulations created a correct pattern of PBS spacing (Fig. 4, B and G). These findings suggest that in-phase genes need to be activated in the root region with low cell division and active growth to create a pattern. In simulated *iaa18/potent* mutant, LR priming occurred continuously, causing fusion of consequent PBS recapitulating the *iaa18/potent* mutant phenotype (Fig. 4, C, E, and G, and movie S5).

We also tested whether the introduction of experimentally derived *ARF7* expression profiles in our model would change its behavior, and we found that the model was robust to fluctuations in ARF7 expression (fig. S9A). Thus, despite the ARF7 oscillations being noisy, the ARF7-IAA18 circuit shows buffering capacity and produces periodically originating PBS with a similar frequency as in the experimental observations (fig. S9B).

Biological clocks can be entrained by external or environmental cues (*30*). As a periodic auxin stimulus has been proposed to regulate the root clock periodicity (*3*, *6*), we performed computer model simulations to test whether a periodic external auxin input into the OZ would entrain the root clock. Simulations of auxin influx into the pericycle showed that the effect on priming is specific to the OZ (cell numbers 20 to 35 from the quiescent center; see data file S3 for details), and thus, influx of auxin at other locations has little or no effect on LR priming frequency. We used 0.01 µM auxin in the

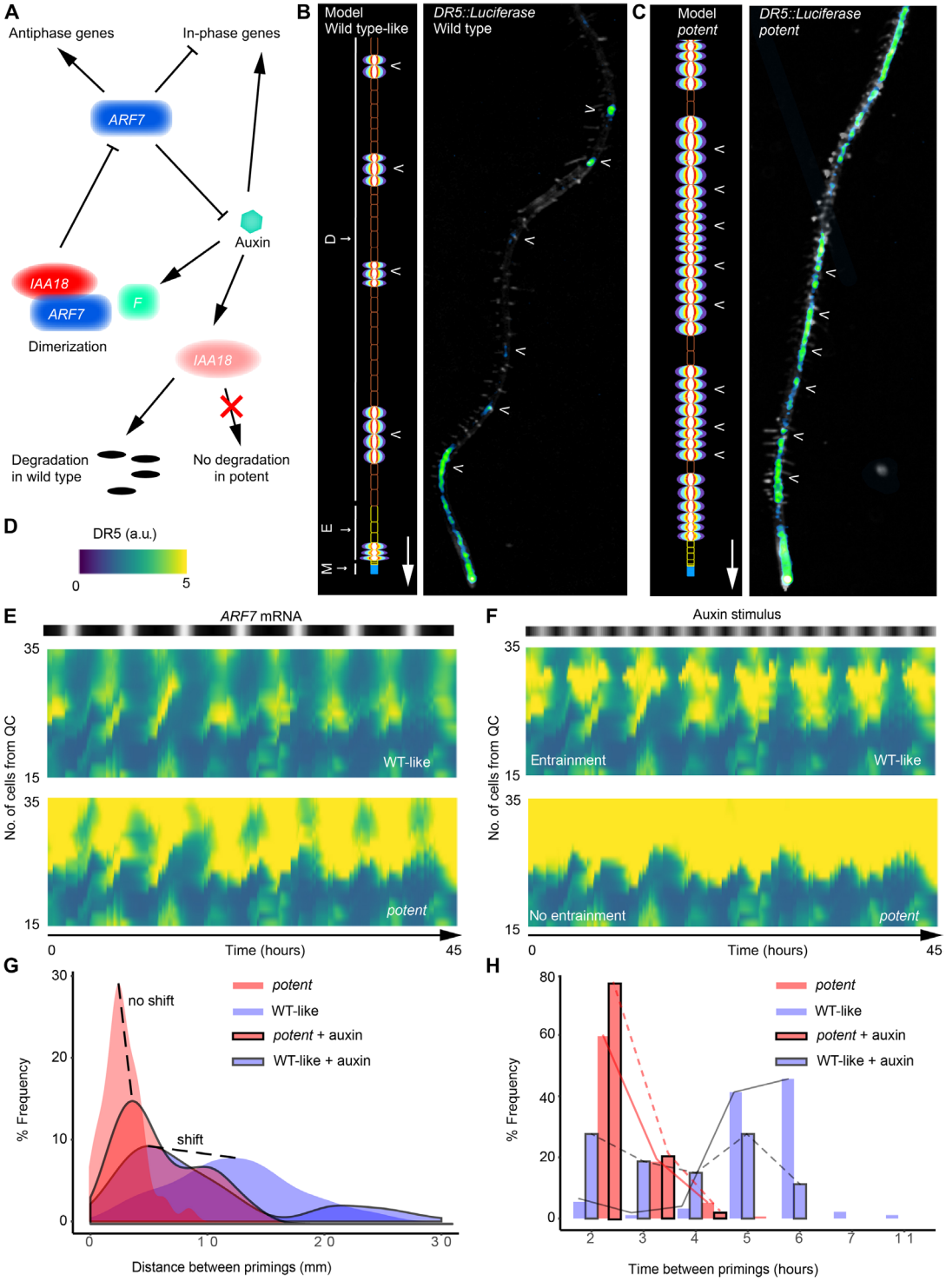

Fig. 4. Multilevel computer model of LR priming predicts ARF7-IAA18/POTENT circuit dynamics in response to a changing environment. (**A**) Schematic representation of the IAA18/POTENT-ARF7 circuit. (**B**) Snapshots of model simulations for the wild-type scenario (left), compared to experimental *DR5::Luciferase* assays (right). M, meristematic root zone; E, elongation root zone; D, differentiation root zone. The pseudocolored ellipse reflects DR5 expression and depicts priming sites and PBS. (**C**) Computer simulations of *iaa18/potent* mutant (left) compared to experimental *DR5::Luciferase* assays in *iaa18/potent* mutant (right). (**D**) Color map for DR5 levels in (E) and (F). a.u., arbitrary units. (**E**) Kymographs of simulated wild type (WT) (top) and *iaa18/potent* mutant (bottom) with oscillating ARF7 mRNA shown on the top bar. DR5 levels are shown across the OZ (~cells 20 to 35). QC, quiescent centre. (**F**) Same as in (E) but with the addition of periodic pulses of external auxin every 3 hours. Note the entrainment of wild type to external auxin stimuli that was absent in *iaa18/potent* mutant simulation. (**G**) Frequency of distance between PBS priming events observed across all simulated scenarios. (**H**) Distribution of oscillatory period between successive priming events. The DR5 threshold for priming was kept the same (4.35) in all simulations.

model simulations, as experimentally, this concentration mimics oscillations of DR5 (*2*). Pulses of auxin every 3 hours led to entrainment in a wild type–like scenario that resulted in increased frequency of priming and reduced PBS spacing (Fig. 4, F to H). However, no entrainment was observed in *iaa18/potent* mutant simulations (Fig. 4, F to H). Gravistimulation has been shown to induce DR5 oscillations and priming (*2*, *31*) and involves auxin transport, which may lead to increased auxin levels in the pericycle (*31*, *32*), reduction in IAA18/POTENT, and, thus, an alteration of clock circuit dynamics. Therefore, we used gravistimulation to test these model predictions. Gravistimulated wild-type roots displayed an increased frequency in PBS formation (fig. S10, A and B), whereas areas with fused PBS were observed in *iaa18/potent* and *arf7* mutants (fig. S10C). Thus, these results are in good agreement with the model predictions, confirming a reduced capacity of *iaa18/potent* and *arf7* mutants to respond to external changes. Last, our model simulations demonstrate that auxin inputs that are in-phase to DR5 amplify the oscillations, resulting in more PBS formation, whereas antiphase auxin inputs did not have a large impact on priming (fig. S9, C and D). This result is in agreement with previous experimental results (*2*) and suggests that external auxin would require coordination with the OZ-located ARF7-IAA18/POTENT circuit to create a pattern. From these observations, we propose a mechanism in which auxin reaching the OZ is interpreted by the ARF7-IAA18 oscillator, which controls auxin through ARF7 in a feedback-dependent manner. Therefore, the oscillations are not merely a readout of external auxin transport or accumulation in the OZ but rather an intrinsic property of a regulable developmental clock.

Biological oscillators such as circadian rhythms and the segmentation clock require negative feedback loops to create robust cyclic patterns (*33*–*36*). The key aspects of our circuit that are necessary for sustainable oscillations are the repressive activity of ARF7 on the in-phase genes and on auxin levels and, predicted by the model, an auxin feedback on ARF7-IAA18/POTENT dimerization, which negatively affects ARF7 activity. Our oscillatory circuit demonstrates central properties of biological clocks as it can buffer molecular noise, creating a periodic pattern and, in addition adapt to external signals, being entrained by persistent fluctuations in hormone levels. When this circuit was implemented in a multilevel model, it generated waves of gene expression traveling across growth domains, a specific characteristic of the root clock, which is shared with the segmentation clock (*1*). Our research demonstrates how an oscillator can be positioned in a growing organ to create a robust pattern of periodic organogenesis.

MATERIALS AND METHODS

Plant material and growth conditions

A. thaliana seeds were surface sterilized with gas chlorine (1% HCl) in a confined environment for 2 hours. After stratification for 1 to 2 days at 4°C, plants were grown on 12 × 12–cm plates with Murashige and Skoog basal medium [MS (2.2 g/liter), 0.05% MES, 1% sucrose, 1% plant agar] in a walk-in custom-made chamber with 16/8-hour light/dark photoperiod at 21° to 23°C. Plants were analyzed at 7 days post imbibition (dpi), except when indicated. Lines previously reported and used in this study were *crane2* (*20*), *iaa28-1* (*37*), the ratiometric R2D2 auxin sensor (*28*) *DR5rev::VENUS-N7* (*38*), *pWOX5::ER-YFP* (*39*), *pSCR::ER-GFP* (*40*), and *DR5::Luciferase, pARF7::Luciferase* and *pLBD16::Luciferase* (*2*). The triply marked line *DR5::Luciferase pWOX5::ER-YFP pSCR::ER-GFP* was generated by crossing the respective parental lines, followed by selection of plants carrying the homozygous markers by means of a fluorescence scope or by luciferase assays. *arf7-1* mutant corresponds to the SALK_040394 line.

Mutagenesis screening and mapping

Seeds from the triply marked line *DR5::Luciferase pWOX5::ER-YFP pSCR::ER-GFP* were mutagenized using ethyl methanesulfonate solution [50 mM EMS and 0.1 M sodium phosphate buffer (pH 5.5)] for 12 hours. About 50 seeds from 2000 independent M2 lines (N = 100,000 seeds) were screened for impairment in LR formation using a fluorescence scope or in luciferase assays. *Potent* was crossed six times with the parental reporter line in *Col-0* ecotype and maintained in heterozygosity as it is a dominant mutation. To map the mutation, *potent* was then crossed five more times with *Ler* ecotype. Approximately 200 seeds generated in the fifth cross were sown, and seedlings with and without *potent* phenotype were collected and frozen at −80°C. Samples were ground with liquid nitrogen using mortar and pestle and incubated with extraction buffer [0.055 M cetyl trimethyl ammonium bromide (CTAB), 1.4 M NaCl, 0.02 M EDTA, and 0.1 M tris-HCl (pH 8.0)] at 60°C for 30 min. Samples were cleaned with equal volume of chloroform and the supernatant precipitated with isopropanol and washed with 70% EtOH before their resuspension in deoxyribonuclease (DNAse)–free water. Samples were sent for sequencing using HiSeq 2000 System [100–base pair (bp) single-end sequencing]. Expression Omnibus accession number for DNA sequences is GSE149996. The SNPtrack pipeline (*41*) was used to identify single variant/nucleotide polymorphisms associated to *Ler* ecotype as well as all the heterozygous mutations present in the *potent* sample. Homozygous *Ler* polymorphisms in the *potent* sample were used to define *Col-0* DNA islands associated to the *potent* phenotype. A heterozygous mutation present in the *potent* sample within the *Col-0* DNA islands identified a dominant mutation in the DII domain of the *IAA18* gene. This mutation was not found in the sample without the *potent* phenotype.

Plasmid construction and plant transformation

Transcriptional and translational fusion lines were generated with the three-fragment Invitrogen Gateway System (Carlsbad, California, United States). *pDONR* plasmids were first generated through BP reaction and then recombined into dpGreenBarT or dpGreenBarT plasmids through LR recombination. To generate *pDONR p4p1* carrying the promoter of *IAA18*, a 3.5-kb promoter region from the start codon of *IAA18* was amplified from Col-0 DNA by polymerase chain reaction (PCR) with the primers 5′-GGGGACAACTTTGTATAGAAAAGTTGCACGACGCCAGTGAAATAGTGT-3′ and 5′-GGGGACTGCTTTTTTGTACAAACTTGGTAGGATTTTTTTTAGAGGAACTACAGAA-3′. To generate *pDONR p4p1* carrying the short version of the *SKP2B* promoter, a 0.5-kb promoter region from the start codon of *SKP2B* was amplified from Col-0 DNA by PCR with the primers 5′-ACAACTTTGTATAGAAAAGTTGAAGCTTTAAAAAATTAACGGATTAGT-3′ and 5′-ACTGCTTTTTTGTACAAACTTGCCTTGAAGCGGTTTCTTTGAT-3′. To generate the *pDONR 221* genomic or coding sequence gene versions of *IAA18* and *potent*, the corresponding regions were amplified from Col-0/*potent* DNA or complementary DNA (cDNA), respectively, by PCR using the primers

5′-GGGGACAAGTTTGTACAAAAAAGCAGGCTGCATGGAGGGTTATTCAAGAAAC-3′ and 5′-GGGG-ACCACTTTGTACAAGAAAGCTGGGTATCTTCTCATTTTCTCTTGCTTAC-3′. To generate *pDONR 221 IAA28*, the coding sequence of *IAA28* was amplified from cDNA using the primers 5′-ACA AGT TTG TAC AAA AAA GCA GGC TCC ATG GAA GAA GAA AAG AGA TTG GAG C-3′ and 5′-AC CAC TTT GTA CAA GAA AGC TGG GTC TTC CTT GCC ATG TTT TCT AGG-3′. To generate *pDONR 221 ARF7*, the coding sequence of *ARF7* was amplified from cDNA using the primers 5′-ACAAGTTTGTACAAAAAAGCAGGCTTTATGAAAGCTCCTTCATCAAATG-3′ and 5′-ACCACTTTGTACAAGAAAGCTGGGTTTCACCGGTTAAACGAAGTGG-3′ for the version with a stop codon and 5′-ACCACT TTGTACAAGAAAGCTGGGTTCCGGTTAAACGAAGTGCTG-3′ for the version without a stop codon. To generate *pDONR 221 NLS*, we used the primers 5′-ACAAGTTTGTACAAAAAAGCAGGCTGCATGGAGCAGAAGCTGATCTC-3′ and 5′-ACCACTTTGTACAAGAAAGCTGGGTAGAATCCTCGAGCGAATTCAT-3′. To generate *pDONR 221 ER*, we used the primers 5′-GGGGACAAGTTTGTACAAAAAAGCAGGCTGCATGAAGACTAATCTTTTTCTC-3′ and 5′-GGGGACCACTTTGTACAAGAAAGCTGGGTAGGCCGAGGATAATGATAGGA-3′. To generate *pDONR p2p3 N-Luciferase*, we used the primers 5′-ACAGCTTTCTTGTACAAAGTGGAA-ATGGAAGACGCCAAAAACATAAAG-3′ and 5′-ACAACTTTGTATAATAAAGTTG-TTATCCATCCTTGTCAATCAAGGC-3′, and to generate *pDONR p2p3 C-Luciferase*, we used the primers 5′-ACAGCTTTC TTGTACAAAGTGGAA-TCCGGTTATGTAAACAATCCGGA-3′ and 5′-ACAACTTTGTATAATAAAGTTG-TTACACGGCGATCTTTCCGC-3′. *pDONR p4p1 pARF7* and *pDONR p2p3 Luciferase* (*2*) and *pDONR p4p1 35S* and *pDONR p2p3 3xYFP* (*42*) were also used. The final constructs were performed using the *IAA18/potent* coding sequence versions except for *pIAA18::IAA18/potent-3xYFP* and split-luciferase fusions, which were made using the genomic versions. The construct pER8:*potent* was generated through traditional LR Gateway recombination using *pDONR p221 potent* (see above) and the *pER8* destination plasmid (*43*). The construct *RecARF7:AraYPET:ARF7* was generated through recombineering (*24*) by fusing the *AraYPET fluorescent protein* gene into the N-terminal part of *ARF7* being carried in the plasmid JATY61O18. The primers used were 5′-TCAGATTATTTATTGGGTTTATTCTTCAGAGAAAGTAAAGTTGAGTGATCGGAGGTGGAGGTGGAGCT-3′ and 5′-AAACCTTCAACAGGATTAGGAGAAACTCCATTTGATGAAGGAGCTTTCATGGCCCCAGCGGCC-′. All constructs were sanger sequenced and transformed into Col-0 or indicated background by floral dip using Agrobacterium strain GV3101. pDEST22/pDEST32 constructs for yeast two hybrid assays and pMal-p2/pGEX-2T constructs for IAA18/potent and ARF7 expression in bacteria were generated through traditional LR Gateway recombination.

Chemical treatments and quantification assays

LR number during growth was quantified on the basis of morphology of emerged LRs or, when indicated, using the markers *pWOX5::ER-YFP* and *pSCR::ER-GFP* in a Leica M205FA fluorescence scope. Mutant or reporter line seedlings were incubated at 4 dpi on MS plates containing 0.25 μM indole-acetic acid (IAA), and the number of LRs was counted at 24, 48, or 72 hours upon treatment. Local auxin treatments upon the OZ were performed at 7 dpi using a 0- to 1-μl micropipette as indicated in (*2*). Mutant or reporter line seedlings were incubated at 4 dpi (or 6 dpi if indicated) on MS plates containing 0.1, 0.5, or 10 μM estradiol or the same estradiol concentrations plus 1 μM IAA for 3 days. To determine the dynamics of ARF7, IAA18, or *potent* protein levels, seedlings from corresponding translational fluorescent lines were added 0.01, 1, or 5 μM IAA or 5 μM IAA plus 5 μM MG132 and mounted on slides for observation under a microscope laser confocal at 1, 2, and 3 hours. Mock or control seedlings were added the equivalent volume or the solvent (dimethyl sulfoxide or ethanol) used to dilute IAA, estradiol, or MG132. To determine the dynamics of *ARF7* transcripts, seedlings from the corresponding *Luciferase* line were incubated on MS plates containing 1 μM IAA or control MS plates for 1 hour, followed by luciferase assays The number of founder cells in mutant lines carrying *pSKP2B0.5:ER-3xmCherry* was determine through the quantification of the number of mCherry-marked cells under confocal laser microscopy.

Luciferase imaging and expression analysis

Plates were sprayed with 1 ml of 2.5 mM potassium luciferine (Gold Biotechnology, St. Louis, Mo., Goldbio.com, cat. no: LUCK-1) and then imaged using a Lumazone CA Automated Chemiluminescence System (Roper Bioscience), NightOwl II (Berthold), or Flumazone (Leica M205FA adapted with Hamamatsu EMCCD X2 camera). Time course analyses were taken using MetaMorph Microscopy Automation Software in a sequence of one bright-field image followed by a 3-min dark interval and then a chemiluminescence image with a 6-min exposure every 20 min for 24 hours. Luciferase expression movies were made by combining the frames, normally three frames/s, using MetaMorph Image Analysis Software. Expression was measured by selecting the region of interest (ROI) and quantifying the analog-digital units per pixel using the MetaMorph Image Analysis Software. When indicated, the luciferase measurements are referred to as the percent change with respect to its own control. The number of PBS was determined using the *DR5::Luciferase* reporter through the quantification of the number of sites with high expression relative to the adjacent regions along the primary root.

Confocal laser microscopy

For confocal laser microscopy, we used a Leica SP8 microscopy with the Leica Application Suite (Las AF Lite) X software or a vertical Zeiss LSM 880 with the ZEN 2.3 SP1 software. Roots were stained with propidium iodide (PI) as indicated. To investigate the expression of the different transcriptional or translational fluorescent protein fusions, we used the standard settings for the corresponding green fluorescent protein (GFP), YFP, or mCherry tags. For R2D2 measurements, all images were taken in the SP8 confocal on counting mode. Venus was excited at 488 nm and detected at 496 to 547 nm, while tdTomato was excited at 561 nm and detected at 565 to 615 nm. In addition, samples were stained with PI, which was excited at 561 nm and detected at 631 to 727 nm. The ratio between red/yellow (mDII/DII) was calculated measuring the mean value of the first six cells through the ROI tool of the Las AF Lite X software.

RNA-seq analyses of the OZ

In the experimental design, the OZ of the control was taken at the minimum expression levels of the oscillation based on the *DR5::Luciferase* reporter and simultaneously for *potent* and *arf7-1*,

without considering the reporter expression, to avoid bias. *DR5::Luciferase* expression was followed using a Lumazone CA Automated Chemiluminescence System (Roper Bioscience). OZs were dissected by using an ophthalmological blade under a dissecting scope and immediately frozen in UltraPure RNA-free water (Invitrogen, Carlsbad, California, United States) using liquid nitrogen. Samples were ground in the same tube with an adapted pestle in the presence of liquid nitrogen, then 0.2 ml of RNAzol (Sigma-Aldrich, Deisenhofen, Germany) was added, and incubated for 15 min at room temperature. Following centrifugation (12,000*g* for 15 min at 4°C), 1.25 µl of 4-bromoanisole (BAM) (Sigma-Aldrich, Deisenhofen, Germany) was added to the supernatant, incubated for 5 min at room temperature, and centrifuged (12,000*g* for 10 min at 4°C). One microliter of Glycoblue (15 mg/ml; Thermo Fisher Scientific, Waltham, Massachusetts, USA) was then added to the supernatant, mixed with 300 µl of isopropanol, and precipitated overnight at 4°C. Samples were centrifuged (12,000*g* for 30 min at 4°C), and the pellet was rinsed with 70% ethanol and air dried. The pellet was resuspended in 8 µl of RNA-free water (Invitrogen, Carlsbad, California, United States) and used for library preparation following the protocol described by Picelli *et al.* (*44*). Libraries were sequenced using HiSeq2000 System (50-bp single-end sequencing). Expression Omnibus accession number for RNA-seq data is GSE149995. Analysis of differentially expressed genes was performed using TopHat and Cufflinks software (*45*). Gene Ontology enrichment analysis was performed using Chip-Enrich (*42*, *43*), and the derived data were represented with the software MeV 4.9 (MultiEexperiment Viewer) (http://mev.tm4.org).

Pull-down assays and Western blot analyses

We used the vectors *pMal-p2* and *pGEX-2T*, carrying *ARF7*, *IAA18*, or *potent* genes to express protein fusions to the maltose binding protein (MBP) and/or glutathione S-transferase (GST) epitopes in *Escherichia coli*. Expression in *E. coli* was induced upon 1 mM isopropyl-β-D-thiogalactopyranoside (IPTG) supplementation, followed by protein extraction through sonication (3× 30-s pulse/30-s pause) in immunoprecipitation (IP) buffer [0.1 M Hepes, 0.3 M KCl, 1 mM phenylmethylsulfonyl fluoride (PMSF), and 1 mM Triton X-100]. Amylose Magnetic Beads (NEB) were used for the purification of MBP-ARF7 and MBP control using recommendations from the manufacturer. Bound MBP-ARF7 or MBP was incubated with GST-IAA18, GST-*potent*, or GST protein extracts at 4°C with agitation for 3 hours. Next, beads were washed five times with IP buffer and used for Western blot assays using anti-MBP or anti-GST (Santa Cruz).

Yeast two-hybrid assay

Saccharomyces cerevisiae strain Hf7c cultures were grown at 28°C in standard or minimal growth media. For direct interaction testing, paired baits (ARF7) and preys (IAA18) in pDEST22/pDEST32 were cotransformed into Hf7c cells. Colonies were selected in solid media containing X-Gal. All experiments were performed in triplicate. Positive and negative controls were IAA18 bait paired with ARF7 prey, and bait or prey paired with the opposing empty vector, respectively. Bait-prey interactions were scored according to β-galactosidase activity.

Statistical analysis

Statistical differences were detected using SPSS Statistics 21 software (IBM). Wald χ^2 was used to analyze homoscedasticity or heteroscedasticity among samples. Homoscedastic groups were analyzed using univariate general linear model (GLM) with least significant difference (LSD) post hoc, whereas heteroscedastic groups were analyzed using generalized linear model (GzLM). For analyses with two homoscedastic samples, we performed Student's *t* test analysis. Significant differences were collected with 5% level of significance.

SUPPLEMENTARY MATERIALS

Supplementary material for this article is available at http://advances.sciencemag.org/cgi/content/full/7/1/eabd4722/DC1

View/request a protocol for this paper from *Bio-protocol*.

REFERENCES AND NOTES

1. M. A. Moreno-Risueno, P. N. Benfey, Time-based patterning in development: The role of oscillating gene expression. *Transcription* **2**, 124–129 (2011).
2. M. A. Moreno-Risueno, J. M. Van Norman, A. Moreno, J. Zhang, S. E. Ahnert, P. N. Benfey, Oscillating gene expression determines competence for periodic *Arabidopsis* root branching. *Science* **329**, 1306–1311 (2010).
3. W. Xuan, H. De Gernier, T. Beeckman, The dynamic nature and regulation of the root clock. *Development* **147**, dev181446 (2020).
4. S. Kircher, P. Schopfer, The plant hormone auxin beats the time for oscillating light-regulated lateral root induction. *Development* **145**, dev169839 (2018).
5. J. M. van Norman, W. Xuan, T. Beeckman, P. N. Benfey, To branch or not to branch: The role of pre-patterning in lateral root formation. *Development* **140**, 4301–4310 (2013).
6. W. Xuan, L. R. Band, R. P. Kumpf, D. Van Damme, B. Parizot, G. De Rop, D. Opdenacker, B. K. Möller, N. Skorzinski, M. F. Njo, B. De Rybel, D. Audenaert, M. K. Nowack, S. Vanneste, T. Beeckman, Cyclic programmed cell death stimulates hormone signaling and root development in *Arabidopsis*. *Science* **351**, 384–387 (2016).
7. I. De Smet, V. Vassileva, B. De Rybel, M. P. Levesque, W. Grunewald, D. Van Damme, G. Van Noorden, M. Naudts, G. Van Isterdael, R. De Clercq, J. Y. Wang, N. Meuli, S. Vanneste, J. Friml, P. Hilson, G. Jürgens, G. C. Ingram, D. Inzé, P. N. Benfey, T. Beeckman, Receptor-like kinase ACR4 restricts formative cell divisions in the *Arabidopsis* root. *Science* **322**, 594–597 (2008).
8. M. Taylor-Teeples, A. Lanctot, J. L. Nemhauser, As above, so below: Auxin's role in lateral organ development. *Dev. Biol.* **419**, 156–164 (2016).
9. G. Wachsman, J. Zhang, M. A. Moreno-Risueno, C. T. Anderson, P. N. Benfey, Cell wall remodeling and vesicle trafficking mediate the root clock in *Arabidopsis*. *Science* **370**, 819–823 (2020).
10. B. De Rybel, V. Vassileva, B. Parizot, M. Demeulenaere, W. Grunewald, D. Audenaert, J. Van Campenhout, P. Overvoorde, L. Jansen, S. Vanneste, B. Möller, M. Wilson, T. Holman, G. Van Isterdael, G. Brunoud, M. Vuylsteke, T. Vernoux, L. De Veylder, D. Inzé, D. Weijers, M. J. Bennett, T. Beeckman, A novel aux/IAA28 signaling cascade activates GATA23-dependent specification of lateral root founder cell identity. *Curr. Biol.* **20**, 1697–1706 (2010).
11. T. Goh, S. Joi, T. Mimura, H. Fukaki, The establishment of asymmetry in *Arabidopsis* lateral root founder cells is regulated by LBD16/ASL18 and related LBD/ASL proteins. *Development* **139**, 883–893 (2012).
12. C. Manzano, E. Ramirez-Parra, I. Casimiro, S. Otero, B. Desvoyes, B. De Rybel, T. Beeckman, P. Casero, C. Gutierrez, J. C. Del Pozo, Auxin and epigenetic regulation of *SKP2B*, an F-box that represses lateral root formation. *Plant Physiol.* **160**, 749–762 (2012).
13. C. K. Worley, N. Zenser, J. Ramos, D. Rouse, O. Leyser, A. Theologis, J. Callis, Degradation of Aux/IAA proteins is essential for normal auxin signalling. *Plant J.* **21**, 553–562 (2000).
14. J. A. Ramos, N. Zenser, O. Leyser, J. Callis, Rapid degradation of auxin/indoleacetic acid proteins requires conserved amino acids of domain II and is proteasome dependent. *Plant Cell* **13**, 2349–2360 (2001).
15. J. M. Guseman, A. Hellmuth, A. Lanctot, T. P. Feldman, B. L. Moss, E. Klavins, L. I. A. Calderón Villalobos, J. L. Nemhauser, Auxin-induced degradation dynamics set the pace for lateral root development. *Development* **142**, 905–909 (2015).
16. P. J. Overvoorde, Y. Okushima, J. M. Alonso, A. Chan, C. Chang, J. R. Ecker, B. Hughes, A. Liu, C. Onodera, H. Quach, A. Smith, G. Yu, A. Theologis, Functional genomic analysis of the *AUXIN/INDOLE-3-ACETIC ACID* gene family members in *Arabidopsis thaliana*. *Plant Cell* **17**, 3282–3300 (2005).
17. S. M. Brady, D. A. Orlando, J.-Y. Lee, J. Y. Wang, J. Koch, J. R. Dinneny, D. Mace, U. Ohler, P. N. Benfey, A high-resolution root spatiotemporal map reveals dominant expression patterns. *Science* **318**, 801–806 (2007).
18. H. Fukaki, S. Tameda, H. Masuda, M. Tasaka, Lateral root formation is blocked by a gain-of-function mutation in the *SOLITARY-ROOT/IAA14* gene of *Arabidopsis*. *Plant J.* **29**, 153–168 (2002).
19. H. Fukaki, Y. Nakao, Y. Okushima, A. Theologis, M. Tasaka, Tissue-specific expression of stabilized SOLITARY-ROOT/IAA14 alters lateral root development in Arabidopsis. *Plant J.* **44**, 382–395 (2005).

20. T. Uehara, Y. Okushima, T. Mimura, M. Tasaka, H. Fukaki, Domain II mutations in CRANE/IAA18 suppress lateral root formation and affect shoot development in *Arabidopsis thaliana*. *Plant Cell Physiol.* **49**, 1025–1038 (2008).
21. M. Salehin, R. Bagchi, M. Estelle, SCFTIR1/AFB-based auxin perception: Mechanism and role in plant growth and development. *Plant Cell* **27**, 9–19 (2015).
22. B. Orosa-Puente, N. Leftley, D. von Wangenheim, J. Banda, A. K. Srivastava, K. Hill, J. Truskina, R. Bhosale, E. Morris, M. Srivastava, B. Kümpers, T. Goh, H. Fukaki, J. E. M. Vermeer, T. Vernoux, J. R. Dinneny, A. P. French, A. Bishopp, A. Sadanandom, M. J. Bennett, Root branching toward water involves posttranslational modification of transcription factor ARF7. *Science* **362**, 1407–1410 (2018).
23. Y. Okushima, H. Fukaki, M. Onoda, A. Theologis, M. Tasaka, ARF7 and ARF19 regulate lateral root formation via direct activation of *LBD/ASL* genes in *Arabidopsis*. *Plant Cell* **19**, 118–130 (2007).
24. R. Zhou, L. M. Benavente, A. N. Stepanova, J. M. Alonso, A recombineering-based gene tagging system for Arabidopsis. *Plant J.* **66**, 712–723 (2011).
25. S. K. Powers, A. S. Holehouse, D. A. Korasick, K. H. Schreiber, N. M. Clark, H. Jing, R. Emenecker, S. Han, E. Tycksen, I. Hwang, R. Sozzani, J. M. Jez, R. V. Pappu, L. C. Strader, Nucleo-cytoplasmic partitioning of ARF proteins controls auxin responses in *Arabidopsis thaliana*. *Mol. Cell* **76**, 177–190.e5 (2019).
26. M. Endo, H. Shimizu, M. A. Nohales, T. Araki, S. A. Kay, Tissue-specific clocks in *Arabidopsis* show asymmetric coupling. *Nature* **515**, 419–422 (2014).
27. W. Xuan, D. Audenaert, B. Parizot, B. K. Möller, M. F. Njo, B. De Rybel, G. De Rop, G. Van Isterdael, A. P. Mähönen, S. Vanneste, T. Beeckman, Root cap-derived auxin pre-patterns the longitudinal axis of the *Arabidopsis* root. *Curr. Biol.* **25**, 1381–1388 (2015).
28. C.-Y. Liao, W. Smet, G. Brunoud, S. Yoshida, T. Vernoux, D. Weijers, Reporters for sensitive and quantitative measurement of auxin response. *Nat. Methods* **12**, 207–210 (2015).
29. I. De Smet, T. Tetsumura, B. De Rybel, N. F. d. Frey, L. Laplaze, I. Casimiro, R. Swarup, M. Naudts, S. Vanneste, D. Audenaert, D. Inzé, M. J. Bennett, T. Beeckman, Auxin-dependent regulation of lateral root positioning in the basal meristem of *Arabidopsis*. *Development* **134**, 681–690 (2007).
30. A. Goldbeter, C. Gérard, D. Gonze, J.-C. Leloup, G. Dupont, Systems biology of cellular rhythms. *FEBS Lett.* **586**, 2955–2965 (2012).
31. M. Laskowski, V. A. Grieneisen, H. Hofhuis, C. A. Ten Hove, P. Hogeweg, A. F. M. Marée, B. Scheres, Root system architecture from coupling cell shape to auxin transport. *PLOS Biol.* **6**, e307 (2008).
32. L. Abas, R. Benjamins, N. Malenica, T. Paciorek, J. Wiśniewska, J. C. Moulinier-Anzola, T. Sieberer, J. Friml, C. Luschnig, Intracellular trafficking and proteolysis of the *Arabidopsis* auxin-efflux facilitator PIN2 are involved in root gravitropism. *Nat. Cell Biol.* **8**, 249 (2006).
33. M. B. Elowitz, S. Leibler, A synthetic oscillatory network of transcriptional regulators. *Nature* **403**, 335–338 (2000).
34. W. Huang, P. Pérez-García, A. Pokhilko, A. J. Millar, I. Antoshechkin, J. L. Riechmann, P. Mas, Mapping the core of the *Arabidopsis* circadian clock defines the network structure of the oscillator. *Science* **336**, 75 (2012).
35. A. Pokhilko, A. P. Fernández, K. D. Edwards, M. M. Southern, K. J. Halliday, A. J. Millar, The clock gene circuit in *Arabidopsis* includes a repressilator with additional feedback loops. *Mol. Syst. Biol.* **8**, 574 (2012).
36. A. B. Webb, A. C. Oates, Timing by rhythms: Daily clocks and developmental rulers. *Dev. Growth Differ.* **58**, 43–58 (2016).
37. L. E. Rogg, J. Lasswell, B. Bartel, A gain-of-function mutation in IAA28 suppresses lateral root development. *Plant Cell* **13**, 465–480 (2001).
38. M. G. Heisler, C. Ohno, P. Das, P. Sieber, G. V. Reddy, J. A. Long, E. M. Meyerowitz, Patterns of auxin transport and gene expression during primordium development revealed by live imaging of the *Arabidopsis* inflorescence meristem. *Curr. Biol.* **15**, 1899–1911 (2005).
39. A. K. Sarkar, M. Luijten, S. Miyashima, M. Lenhard, T. Hashimoto, K. Nakajima, B. Scheres, R. Heidstra, T. Laux, Conserved factors regulate signalling in *Arabidopsis thaliana* shoot and root stem cell organizers. *Nature* **446**, 811–814 (2007).
40. L. Di Laurenzio, J. Wysocka-Diller, J. E. Malamy, L. Pysh, Y. Helariutta, G. Freshour, M. G. Hahn, K. A. Feldmann, P. N. Benfey, The SCARECROW gene regulates an asymmetric cell division that is essential for generating the radial organization of the *Arabidopsis* root. *Cell* **86**, 423 (1996).
41. I. Leshchiner, K. Alexa, P. Kelsey, I. Adzhubei, C. A. Austin-Tse, J. D. Cooney, H. Anderson, M. J. King, R. W. Stottmann, M. K. Garnaas, S. Ha, I. A. Drummond, B. H. Paw, T. E. North, D. R. Beier, W. Goessling, S. R. Sunyaev, Mutation mapping and identification by whole-genome sequencing. *Genome Res.* **22**, 1541–1548 (2012).
42. H. Tsukagoshi, W. Busch, P. N. Benfey, Transcriptional regulation of ROS controls transition from proliferation to differentiation in the root. *Cell* **143**, 606–616 (2010).
43. A. Coego, E. Brizuela, P. Castillejo, S. Ruíz, C. Koncz, J. C. del Pozo, M. Piñeiro, J. A. Jarillo, J. Paz-Ares, J. León; TRANSPLANTA Consortium, The TRANSPLANTA collection of Arabidopsis lines: A resource for functional analysis of transcription factors based on their conditional overexpression. *Plant J.* **77**, 944–953 (2014).
44. S. Picelli, O. R. Faridani, A. K. Björklund, G. Winberg, S. Sagasser, R. Sandberg, Full-length RNA-seq from single cells using Smart-seq2. *Nat. Protoc.* **9**, 171–181 (2014).
45. C. Trapnell, A. Roberts, L. Goff, G. Pertea, D. Kim, D. R. Kelley, H. Pimentel, S. L. Salzberg, J. L. Rinn, L. Pachter, Differential gene and transcript expression analysis of RNA-seq experiments with TopHat and Cufflinks. *Nat. Protoc.* **7**, 562–578 (2012).
46. L. Keviczky, R. Bars, J. Hetthéssy, C. Bányász, Introduction to MATLAB, in *Control Engineering: MATLAB Exercises* (Springer, Singapore, 2019).
47. R. R Development Core Team, R: A Language and Environment for Statistical Computing. R Foundation for Statistical Computing. (2011).
48. C. Ginestet, ggplot2: Elegant graphics for data analysis. *J. R. Stat. Soc. A. Stat. Soc.* **174**, 245–246 (2011).
49. B. Carpenter, A. Gelman, M. D. Hoffman, D. Lee, B. Goodrich, M. Betancourt, M. Brubaker, J. Guo, P. Li, A. Riddell, Stan: A probabilistic programming language. *J. Stat. Softw.* **76**, 1–32 (2017).
50. P.-C. Bürkner, brms: An R package for bayesian multilevel models using stan. *J. Stat. Softw.* **80**, 1–28 (2017).
51. G. T. S. Beemster, T. I. Baskin, Analysis of cell division and elongation underlying the developmental acceleration of root growth in *Arabidopsis thaliana*. *Plant Physiol.* **116**, 1515–1526 (1998).
52. F. Bizet, I. Hummel, M.-B. Bogeat-Triboulot, Length and activity of the root apical meristem revealed in vivo by infrared imaging. *J. Exp. Bot.* **66**, 1387–1395 (2015).
53. X. Yang, G. Dong, K. Palaniappan, G. Mi, T. I. Baskin, Temperature-compensated cell production rate and elongation zone length in the root of *Arabidopsis thaliana*. *Plant Cell Environ.* **40**, 264–276 (2017).
54. V. V. Mironova, N. A. Omelyanchuk, G. Yosiphon, S. I. Fadeev, N. A. Kolchanov, E. Mjolsness, V. A. Likhoshvai, A plausible mechanism for auxin patterning along the developing root. *BMC Syst. Biol.* **4**, 98 (2010).
55. K. Wabnik, K. Wabnik, J. Kleine-Vehn, J. Balla, M. Sauer, S. Naramoto, V. Reinöhl, R. M. H. Merks, W. Govaerts, J. Friml, Emergence of tissue polarization from synergy of intracellular and extracellular auxin signaling. *Mol. Syst. Biol.* **6**, 447 (2010).

Acknowledgments

Funding: This work was funded by the Ministerio de Economía y Competitividad of Spain (MINECO) and/or the ERDF (BFU2016-80315-P to M.A.M.-R., BIO2017-82209-R to J.C.d.P., and TIN2016-81079-R to A.R.-P.), the Comunidad de Madrid and/or ERDF and ESF (2017-T1/BIO-5654 to K.W. and S2017/BMD-3691 to A.R.-P.), the Howard Hughes Medical Institute and the NIH (R35-GM131725 to P.N.B.), the Fonds Wetenschappelijk Onderzoek (FWO Flanders) (G022516N, G020918N, and G024118N to T.B.), and the "Severo Ochoa Program for Centres of Excellence in R&D" from the Agencia Estatal de Investigacion of Spain [SEV-2016-0672 (2017–2021)] to K.W., P.P.-G., and M.A.M.-R. through CBGP. M.M. was supported by a postdoctoral contract associated to SEV-2016-0672, E.B.-A. by Ayudante de Investigacion contract PEJ-2017-AI/BIO-7360 from the Comunidad de Madrid, A.S.-C. and L.S.-R. by FPI contracts from MINECO (BES-2014-068852 and BES-2017-080155, respectively), J.C. by a Juan de la Cierva contract from MINECO (FJCI-2016-28607), P.P.-G. by a Juan de la Cierva contract from MINECO (FJCI-2015-24905) and Programa Atraccion Talento from Comunidad Madrid (2017-T2/BIO-3453), A.S. by a Torres Quevedo contract from MINECO (PTQ-15-07915), and K.W. by program PGC2018-093387-A-I00 from the Ministerio de Ciencia e Innovacion (MICIU).
Author contributions: J.P.-R., E.B.-A., G.W., A.S.-C., H.D.G., J.C., P.P.-G., I.G., A.S., and L.S.-R. contributed to the acquisition and analyses of data. M.A.M.-R., J.P.-R., E.B.-A., G.W., J.C.d.P., P.N.B., H.D.G., and T.B. contributed to the conception and design of the experiments. M.R., M.M., K.W., and A.R.-P. performed the modeling and simulations. M.A.M.-R., K.W., M.R., M.M., J.P.-R., and E.B.-A. wrote the manuscript. P.N.B., J.C.d.P., and T.B. revised the manuscript.
Competing interests: P.N.B. is the co-founder and Chair of the Scientific Advisory Board of Hi Fidelity Genetics Inc., a company that works on crop root growth. The authors declare that they have no other competing interests. **Data and materials availability:** Materials will be provided through material transfer agreements. Expression Omnibus accession number for DNA mapping sequences is GSE149996 and for RNA-seq data is GSE149995. All data needed to evaluate the conclusions in the paper are present in the paper and/or the Supplementary Materials. Additional data related to this paper may be requested from the authors.

Submitted 23 June 2020
Accepted 6 November 2020
Published 1 January 2021
10.1126/sciadv.abd4722

Citation: J. Perianez-Rodriguez, M. Rodriguez, M. Marconi, E. Bustillo-Avendaño, G. Wachsman, A. Sanchez-Corrionero, H. De Gernier, J. Cabrera, P. Perez-Garcia, I. Gude, A. Saez, L. Serrano-Ron, T. Beeckman, P. N. Benfey, A. Rodríguez-Patón, J. C. del Pozo, K. Wabnik, M. A. Moreno-Risueno, An auxin-regulable oscillatory circuit drives the root clock in *Arabidopsis*. *Sci. Adv.* **7**, eabd4722 (2021).

An auxin-regulable oscillatory circuit drives the root clock in *Arabidopsis*

Juan Perianez-Rodriguez, Marcos Rodriguez, Marco Marconi, Estefano Bustillo-Avendaño, Guy Wachsman, Alvaro Sanchez-Corrionero, Hugues De Gernier, Javier Cabrera, Pablo Perez-Garcia, Inmaculada Gude, Angela Saez, Laura Serrano-Ron, Tom Beeckman, Philip N. Benfey, Alfonso Rodríguez-Patón, Juan Carlos del Pozo, Krzysztof Wabnik and Miguel A. Moreno-Risueno

Sci Adv **7** (1), eabd4722.
DOI: 10.1126/sciadv.abd4722